Taylor & Francis
Taylor & Francis Group

Robust optimization with time-dependent uncertainty in radiation therapy

Omid Nohadani [a] and Arkajyoti Roy[a,b]

[a]Department of Industrial Engineering and Management Sciences, Northwestern University, Evanston, IL, USA; [b]Department of Applied Statistics and Operations Research, Bowling Green State University, Bowling Green, OH, USA

ABSTRACT

In the recent past, robust optimization methods have been developed and successfully applied to a variety of single-stage problems. More recently, some of these approaches have been extended to multi-stage settings with fixed uncertainties. However, in many real-world applications, uncertainties evolve over time, rendering the robust solutions suboptimal. This issue is particularly prevalent in medical decision making, where a patient's condition can change during the course of the treatment. In the context of radiation therapy, changes in cell oxygenation directly affect the response to radiation. To address such uncertain changes, we provide a general robust optimization framework that incorporates time-dependent uncertainty sets in a tractable fashion. Temporal changes reside within a cone, whose projection at each step yields the current uncertainty set. We develop conic robust two-stage linear problems and provide their robust counterparts for uncertain constraint parameters, covering the range of radiation therapy problems. For a clinical prostate cancer case, the time-dependent robust approach improves the tumor control throughout the treatment, as opposed to current methods that lose efficacy at some stage. We show that this advantage does not bear additional risks compared to current clinical methods. For intermediate diagnostics, we provide the optimal observation timing that maximizes the value of information. While these findings are relevant to clinical settings, they are also general and can be applied to a broad range of applications; e.g., in maintenance scheduling.

1. Introduction

In the presence of uncertainties, solutions from deterministic optimization models can lead to undesirable and impracticable strategies. When uncertainties can be described by probability distributions, stochastic optimization (SO) can be employed (Dantzig, 1955; Birge and Louveaux, 2011). However, in many instances, the nature of the uncertainties is not probabilistic, but rather deterministic or even adversarial. For such cases, the uncertainties are considered to be contained within a set, over which robust optimization (RO) is performed.

The success of an RO approach is chiefly attributed to its computation tractability. In this context, tractability refers to solving a problem of a realistic size in practical times. Ben-Tal *et al.* (2009) demonstrate that a robust linear problem (LP) can be reformulated via its robust counterpart (RC) which is tractable, whenever the convex uncertainty set itself is tractable; i.e., the problem can be expressed as a system of finite number of convex constraints. Therefore, the tractability of the RC decisively depends on the geometry of the uncertainty set. LP models employing various uncertainty sets, including ellipsoidal, polyhedral, and general norms, are computationally tractable in most cases. For further details on theory and application of RO in the LP domain, see Ben-Tal and Nemirovski (1999) and Bertsimas

et al. (2011). For nonconvex approaches, see Bertsimas *et al.* (2010b).

In multi-stage settings, robust solutions can be either time-independent or time-dependent. Time-independent solutions imply that all decisions are taken at once, whereas time-dependent solutions delay some decisions into the future. A time-dependent robust LP can be expressed as

$$\left\{ \min_{\mathbf{x}} \quad \mathbf{c}^{t'}\mathbf{x}^t : A^t\mathbf{x}^t \geq \mathbf{b}^t, \qquad A^t \in \mathcal{U} \right\}, \qquad (1)$$

where $\mathbf{c}^t \in \mathbb{R}^n$ are objective coefficients, $A^t \in \mathbb{R}^{m \times n}$ are constraint coefficients, and $\mathbf{b}^t \in \mathbb{R}^m$ are thresholds parameters. Equation (1) optimizes decision variables $\mathbf{x} = (\mathbf{x}^1, \dots, \mathbf{x}^T)'$ with $\mathbf{x}^t \in \mathbb{R}^n$ based on the uncertain $A^t \in \mathcal{U}$, even in the worst case.

When intermediate observations are accommodated, the time-dependent solution space can be separated into solutions that are needed in the first-stage, prior to any observation, and solutions that are required in future stages; i.e., post-observation. In such formulations, the decision maker can adapt the future-stage decisions to the realizations after the previous stage. In the context of SO, recourse variables are used to adapt to first-stage realizations (Dantzig and Madansky, 1961). However, for large-scale problems, stochastic models become intractable, hence become limited in applicability (Shapiro and Nemirovski, 2005).

The adaptive robust optimization (ARO) approach is an alternative way of incorporating additional information. However, exact ARO methods remain computationally intractable, similar to stochastic methods (Guslitser, 2002). To induce tractability, approximations of the exact ARO are proposed. Ben-Tal *et al.* (2004) develop an affine adjustable robust model for a two-stage problem, where the second-stage solutions are affine functions of the first-stage solutions and realized uncertainties. In fact, in many real-world applications, the affine approximations have proven to be realistic and, hence, can be considered as a tractable method for computing ARO solutions (Calafiore and Campi, 2005; Mani *et al.*, 2006; Ordóñez and Zhao, 2007; Mudchanatongsuk *et al.*, 2008). Bertsimas and Caramanis (2010) introduce the finite adaptable model, which provides the difference between a non-adaptive model and an exact ARO. Such models compute a finite number of contingency plans based on possible realization scenarios of the uncertainty. The resulting finite model is computationally efficient for problems with a small number of dimensions and scenarios. Additionally, tractability is also maintained for the ARO when the uncertainty is assumed to take values in the finite set with lower cardinality (Bertsimas and Caramanis, 2010). For example, when the uncertainty is bounded by the l_1 norm, the ARO can be computed efficiently (Men *et al.*, 2014). For larger problems, Bertsimas and Caramanis (2010) show that, infinitely adaptable models, even a two-adaptable (with two contingency plans) optimization problem is intractable. These continuous uncertainty sets cause the problem to be NP-hard. In the context of energy optimization, Lorca and Sun (2015) introduced the concept of time into RO via a dynamic optimization model, which is computationally efficient, but requires a sizable number of assumptions (as typically for dynamic programming). To the best of our knowledge, all previous approaches do not model the uncertainty as a function of time but rather use different and fixed sets for different times. However, time-dependent uncertainty sets occur in various real-world applications, where using static sets may not capture the dynamics of the problem or turn sub-optimal at later time periods.

In this work, we extend concepts of ARO to time-dependent uncertainty sets. Observations during the process establish the notion of time. The uncertainty grows as the updated information ages. The goal is to provide solutions that are robustly optimized at each stage while mitigating the price of robustness. Furthermore, we seek to reduce the size of the problem by considering only those solutions that are relevant to each time period, making the problem computationally more efficient. Specifically, we focus on robust linear problems.

1.1. Contributions

We propose a two-stage robust optimization model for time-dependent uncertainties that can be solved efficiently for large problems with low dimensional uncertainty sets. The model produces "here-and-now" solutions for the entire process at the beginning, in anticipation of possible changes. An observation into the system concludes the first stage and reveals the accurate levels of the previously considered uncertainties. Based on this information, the adapted second-stage solutions are implemented. Specifically, we:

- construct the time-dependent uncertainty set using a conic geometry;
- formulate the conic robust two-stage LP and its robust counterpart;
- provide a framework for an optimal observation schedule;
- model changes to cell reoxygenation in radiation therapy; and
- evaluate this model on a prostate cancer case to illustrate potential clinical impact.

1.2. Notation

Throughout this article, we denote vectors with bold type and matrices with uppercase letters. Time is denoted with t and the point of observation is τ.

The rest of the article is outlined as follows: in Section 2, the uncertainty cone is constructed based on uncertain parameters of the LP. In Section 3, the two-stage LP and its counterparts are discussed. The optimal observation policy is developed in Section 4. A hypoxia-based radiation therapy planning problem, using the two-stage LP, is presented in Section 5 along with the results of a clinical prostate case.

2. Time-dependent uncertainty model

For the sake of generality, we denote A^t as $A(t)$ since the coefficients of A may have a functional dependence on t. Furthermore, we consider two forms of uncertainty on $A(t)$, namely the general norm uncertainty on all elements and the row-wise uncertainty. For the norm uncertainty, all elements $a_{i,j}$ in matrix A are considered to reside in a convex compact uncertainty set $\mathcal{U}$. In the row-wise uncertainties, the ith row elements $a_{i,j}$ are in $\mathcal{U}_i$ over all columns j. Note that the row-wise setting provides flexibility in modeling uncertainty over different dimensions. Since it can be considered as a subset of the general norm uncertainty, we discuss the general norm first to arrive at the main conclusions, before specifying for the row-wise setting. We do not consider the case of column-wise uncertainty, because it assumes extremely conservative scenarios that are highly unlikely to occur in reality (Ben-Tal and Nemirovski, 1999).

In this section, we address uncertainties that can change as time evolves. In fact, the uncertainty in $A(t)$ grows as the initial accurate information ages and becomes more vague (the intuition for the row-wise uncertainty is analogous). For this, we can refine the space as a parameter-time space (A, t), which leads to a time-dependent uncertainty set $\mathcal{U}(t)$. A natural description of the temporal boundaries of $\mathcal{U}(t)$ is a higher-dimensional horizon, within which uncertainties are considered. If we regard the realization of (A, t) as an "event" in the parameter-time space, the notion of the event horizon from the theory of relativity in physics, only within which events can be observed, offers an analogous description. Correspondingly, we can model the event horizon through a conic geometry, within which uncertainties can be realized, as illustrated in Fig. 1 (top).

Consider the uncertainty cone to be initialized at the start of the process as $A(t = 0)$ based on measurements. As time evolves, $A(t > 0)$ can become more uncertain because the initial information grows more distant. In other words, the separation
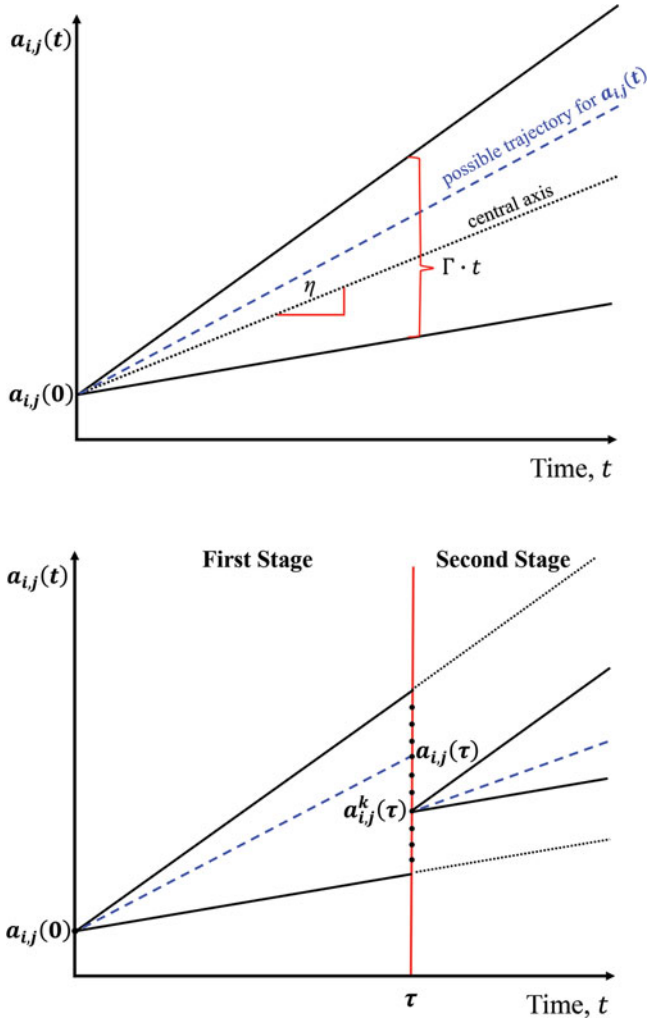
Figure 1. Top: Uncertainty cone without observation. Bottom: Re-initialized cone with accurate observation.

from $A(0)$ causes an enlargement of the uncertainty set in time. We can model this via an uncertainty cone that widens in time to capture the enlarged set. With this description, at any time t, the realized uncertainty set $\mathcal{U}(t)$ is the n-dimensional projection of this $n + 1$ dimensional cone.

For the general p-norm, the $n + 1$ dimensional uncertainty cone can be expressed as,

$$\mathcal{U}(t) = \{A(t) \mid \|\text{vec}\,(A(t)) - \text{vec}\,(A(0)) + \eta(t)\|_p \leq \Gamma t\}, \quad (2)$$

and the row-wise uncertainty as,

Here, $\text{vec}(A(t))$ denotes that the successive rows of matrix $A(t)$ are appended to form a vector. is the vector obtained by stacking the rows of matrix $A(t)$ on top of each other. $\eta_i(t)$ controls the tilt of the cone (symmetry axis of the cone) and is the same for all i with $\eta_i(0) = \mathbf{0}$. We use the p-norm, denoted by $\|\cdot\|_p$, to conserve the generality of the approach. Specific norms are discussed in Section 3. For the row-wise uncertainty, $\mathbf{a}_i(t)$ is the vector of coefficients in row i, and Δ_i is a vector that controls the skew of the i-th uncertainty set. Γ is a scalar that controls the rate of change (cone opening). A conservative decision maker may prefer a large Γ to capture all realistic scenarios. The choice of Γ can also be motivated by historical data and experience about the process. For the radiation therapy discussion in Section 5, we will discuss the details of the choice of Γ.

The size of $\mathcal{U}(t)$ grows as time evolves, resulting in potentially over-conservative solutions. To reduce this cost of robustness, practitioners may allow an intermediate observation at $t = \tau$ to update the information. To model this, $\mathcal{U}(t)$ will be adapted at τ.

2.1. Time-dependent uncertainty set

At the observation point τ, the parameters are measured accurately. This observed and certain value $A_{\text{obs}}(\tau)$ may not match $A(t = \tau)$, which is based on the forecasted and uncertain progression. This deviation, however, is bound by $\mathcal{U}(\tau)$ and is in the set $\{\|\text{vec}\,(A_{\text{obs}}(\tau)) - \text{vec}\,(A(0)) + \eta(\tau)\|_p \leq \Gamma \tau\}$. In principle, there can be infinitely many possible realizations of this deviation within the interval $[-\Gamma\tau, +\Gamma\tau]$, which can cause the problem to become intractable. In many real-world settings, however, observations are measured in increments of the underlying units (e.g., for radiation in cGy). We therefore discretized possible values of $A_{\text{obs}}(\tau)$ for a finite number of $k = 1, \ldots, K$ scenarios, denoted by $A^k(\tau)$. The second-stage structure of the problem (after the observation) remains the same as before, but now with the new and accurately measured values $A^k(\tau)$. As a result, the uncertainty set of the second stage can be decomposed into K scenarios. This allows us to maintain the tractability of the problem, which is NP-hard otherwise (Bertsimas and Caramanis, 2010). Figure 1 (bottom) illustrates a two-dimensional cone, where the observation takes place at τ. In comparison, the cross section of the original cone at $t > \tau$ will always be larger (dotted extension) than the cross-section of the re-initialized cone. Therefore, the uncertainty set size will be smaller, when observation is permitted.

The time-dependent uncertainty cone $\mathcal{U}^k(t)$ can be expressed for the general norm as,

$$\mathcal{U}^k(t) = \left\{ A(t) \middle| \begin{array}{ll} \|\text{vec}\,(A(t)) - \text{vec}\,(A(0)) + \eta(t)\|_p \leq \Gamma t & \forall t < \tau, \\ \|\text{vec}(A(t)) - \text{vec}(A^k(\tau)) + \eta(t - \tau)\|_p \leq \Gamma(t - \tau) & \forall t \geq \tau \end{array} \right\}, \quad (4)$$

and the row-wise uncertainty as,

$$\mathcal{U}^k(t) = \left\{ \mathbf{a}_i(t) \middle| \begin{array}{ll} \Delta_i \|\mathbf{a}_i(t) - \mathbf{a}_i(0) + \eta_i(t)\|_p \leq \Gamma t & \forall t < \tau, \\ \Delta_i \|\mathbf{a}_i(t) - \mathbf{a}_i^k(\tau) + \eta_i(t - \tau)\|_p \leq \Gamma(t - \tau) & \forall t \geq \tau \end{array} \right\}. \quad (5)$$

and for the row-wise uncertainty as,

$$\mathcal{U}_i(t) = \{\mathbf{a}_i(t) \mid \Delta_i \| (\mathbf{a}_i(t)) - (\mathbf{a}_i(0)) + \eta_i(t)\|_p \leq \Gamma_i t\}. \quad (3)$$

Analogous to the element-wise observation $A_{\text{obs}}^k(\tau)$, the row-wise observed parameters also depend on the elapsed time as $\mathbf{a}_{\text{obs},i}(\tau)$ and can take finitely many values $\mathbf{a}_i^k(\tau)$. We seek to find

an optimal solution that is inherently robust within these varying uncertainty sets. For this, we next discuss the corresponding approach.

3. Conic robust two-stage linear model

We construct the robust formulation by incorporating the general norm uncertainty set (Eq. (4)) into the uncertain LP (Eq. (4)). Since the time-dependent uncertainty is decomposable in k, the conic robust two-stage LP for scenario k is expressed as,

$$\min_{\mathbf{x}^k} \sum_{t=1}^{T} \mathbf{c}(t)' \mathbf{x}^k(t)$$

$$\text{s.t. } A(t)\mathbf{x}^k(t) \leq \mathbf{b}(t) \quad A(t) \in \mathcal{U}^k(t), \forall t$$

$$\sum_{t=1}^{T} G\mathbf{x}^k(t) \leq \mathbf{g} \tag{6}$$

The symmetry of $\mathcal{U}^k(t)$, (i.e., same form before and after the observation), allows for a compact formulation with $x^k(t) = x(t)$ for $t < \tau$. Note that the first constraint has to hold for each time period, while the uncertainty set evolves. The second constraint connects all time periods over the fixed budget $\mathbf{g}$ and the certain parameters G. The following proposition leads to a tractable solution of the conic robust two-stage LP (Eq. (6)).

Proposition 1. *The robust counterpart to Problem (6) under the general norm uncertainty (4) is given by,*

$$\min_{\mathbf{x}^k} \sum_{t=1}^{T} \mathbf{c}(t)' \mathbf{x}^k(t)$$

$$\text{s.t. } (\mathbf{a}_i(0) + \boldsymbol{\eta}(t))' \mathbf{x}(t) + \|\mathbf{x}_i(t)\|_q \Gamma t \leq b_i(t) \quad \forall t < \tau, \forall i$$

$$\left(\mathbf{a}_i^k(\tau) + \boldsymbol{\eta}(t - \tau)\right)' \mathbf{x}^k(t) + \|\mathbf{x}_i^k(t)\|_q \Gamma(t - \tau)$$

$$\leq b_i(t) \quad \forall t \geq \tau, \forall i,$$

$$\sum_{t=1}^{T} G\mathbf{x}^k(t) \leq \mathbf{g}, \tag{7}$$

where rows $\mathbf{a}_i^k(\tau)$ take the observed values at scenario k and $\| \cdot \|_q$ is the dual of the p-norm with $1 = p^{-1} + q^{-1}$. Here, $\mathbf{x}_i^k(t) \in \mathbb{R}^{(m \cdot n) \times 1}$ is a vector that contains zero everywhere, except for elements $n(i - 1) + 1$ through $n \cdot i$, which are filled with the vector $\mathbf{x}^k(t) \in \mathbb{R}^{n \times 1}$ and $\mathbf{x}^k(t) = \mathbf{x}(t)$ for $t < \tau$.

Proof. For $t < \tau$, let $\mathbf{y} = \frac{\text{vec}(A(t)) - \text{vec}(A(0)) + \boldsymbol{\eta}(t)}{\Gamma \cdot t}$. Then, we obtain a single-variable uncertainty set $\mathcal{U}(t) = \{\mathbf{y} \mid \|\mathbf{y}\|_p \leq 1\}$. Thus, using the definition of the dual norm $\|\mathbf{s}\|^* \equiv \max_{\{\|\mathbf{y}\| \leq 1\}} \mathbf{s}'\mathbf{y}$, we can write the uncertain constraint i (row i of matrix $A(t)$) as,

$$\max_{\{\text{vec}(A(t)) \in \mathcal{U}(t)\}} \{\mathbf{a}_i(t)'\mathbf{x}(t)\}$$

$$= \max_{\{\text{vec}(A(t)) \in \mathcal{U}(t)\}} \{\text{vec}(A(t))' \mathbf{x}_i(t)\}$$

$$= \max_{\|\mathbf{y}\|_p \leq 1} \{(\text{vec}(A(0)) + \boldsymbol{\eta}(t))' \mathbf{x}_i(t) + \Gamma t \mathbf{y}'\mathbf{x}_i(t)\}$$

$$= (\mathbf{a}_i(0) + \boldsymbol{\eta}(t))' \mathbf{x}(t) + \Gamma t \max_{\{\|\mathbf{y}\|_p \leq 1\}} \{\mathbf{y}'(\mathbf{x}_i(t))\}$$

$$= (\mathbf{a}_i(0) + \boldsymbol{\eta}(t))' \mathbf{x}(t) + \Gamma t \|\mathbf{x}_i(t)\|_q.$$

For $t \geq \tau$, using the dual norm,

$$\max_{\{\text{vec}(A(t)) \in \mathcal{U}^k(t)\}} \{\mathbf{a}_i(t)'\mathbf{x}(t)\}$$

$$= \left(\mathbf{a}_i^k(\tau) + \boldsymbol{\eta}(t - \tau)\right)' \mathbf{x}^k(t) + \Gamma(t - \tau)\|\mathbf{x}_i^k(t)\|_q$$

computes the robust counterpart from Proposition 1.   □

This extends the proof by Bertsimas *et al.* (2004) to time-dependent settings with observation by separating the period $t < \tau$ from the $t \geq \tau$.

For row-wise uncertainty, the following corollary provides the RC.

Corollary 1. *The robust counterpart to the conic robust Eq. (6) under a row-wise uncertainty is,*

$$\min_{\mathbf{x}^k} \sum_{t=1}^{T} \mathbf{c}(t)' \mathbf{x}^k(t)$$

$$\text{s.t. } \left(\mathbf{a}_i(0) + \boldsymbol{\eta}_i(t)\right)' \mathbf{x}(t) + \Delta_i \|\mathbf{x}(t)\|_q \Gamma_i t \leq b_i(t) \quad \forall t < \tau, \forall i$$

$$\left(\mathbf{a}_i^k(\tau) + \boldsymbol{\eta}_i(t - \tau)\right)' \mathbf{x}^k(t) + \Delta_i \|\mathbf{x}^k(t)\|_q \Gamma_i(t - \tau)$$

$$\leq b_i(t) \forall t \geq \tau, \forall i \sum_{t=1}^{T} G\mathbf{x}^k(t) \leq \mathbf{g}. \tag{8}$$

Note that the main difference between the robust counterparts of Eqs. (7) and (8) is that the row-wise setting allows for more flexibility via the skew factor Δ_i for dimension i. This degree of freedom allows us to model individual growth of uncertainty of each parameter dimension. Furthermore, for both uncertainty types, specific instances of the p-norm can be used. Note that l_1 and l_∞ norm are dual to each other and l_2 norm is self-dual.

The structure of the reformulation can also be translated to the case of right-hand side (RHS) uncertainties in vector $\mathbf{b}(t)$, which can evolve over time. Ben-Tal *et al.* (2009) have shown that a RHS uncertainty can be transformed into a left-hand-side uncertainty. In the following, we extend this result to time-dependent uncertainties for completeness of the exposition and will use it in the discussion of radiation therapy planning.

3.1. Right-hand side uncertainty

Analogously, $\mathbf{b}(t)$ can evolve over time and we assume that $\mathbf{b}(t = \tau)$ is accurately observed within a discretized set. The uncertain constraint in Eq. (6) takes the form

$$A(t)\mathbf{x}^k(t) \geq \mathbf{b}(t) \qquad \mathbf{b}(t) \in \mathcal{U}^k(t), \forall t. \tag{9}$$

Proposition 2. *If the general norm right-hand side uncertainty for $b_i(t) \in \mathcal{U}^k(t)$ over all constraints i is given by*

$$\mathcal{U}^k(t)$$

$$= \left\{ b_i(t) \middle| \begin{cases} \|\mathbf{b}(t) - \mathbf{b}(0) + \boldsymbol{\eta}(t)\|_p \leq \Gamma t & \forall t < \tau, \\ \|\mathbf{b}(t) - \mathbf{b}^k(\tau) + \boldsymbol{\eta}(t - \tau)\|_p \leq \Gamma(t - \tau) & \forall t \geq \tau \end{cases} \right\},$$

$$\tag{10}$$

with the observed $\mathbf{b}^k(\tau)$, then the robust counterpart of Eq. (9) can be expressed as

$$\mathbf{a}_i(t)'\mathbf{x}(t) \geq b_i(0) + \boldsymbol{\eta}(t) + \Gamma t \qquad \forall t < \tau, \forall i,$$

$$\mathbf{a}_i(t)'\mathbf{x}^k(t) \geq b_i^k(\tau) + \boldsymbol{\eta}(t - \tau) + \Gamma(t - \tau) \quad \forall t \geq \tau, \forall i. \tag{11}$$

Proof. We divide the proof for the period before and after the observation. For $t < \tau$, let $\mathbf{y} = \frac{b(t)-b(0)+\eta(t)}{\Gamma t}$ and $\mathbf{z}_i$ be a vector of the same length as $\mathbf{b}(t)$ filled with zeros, except for the element i that is one. Using the dual norm, we can write for the constraint i

$$\max_{\{b_i(t) \in \mathcal{U}(t)\}} b_i(t) = \max_{\{\mathbf{y}|\ \|\mathbf{y}\|_q \leq 1\}} \left(\Gamma t\mathbf{y} + \mathbf{b}(0) + \boldsymbol{\eta}(t)\right)' \mathbf{z}_i(t)$$
$$= b_i(0) + \eta_i(t) + \Gamma t\|\mathbf{z}_i(t)\|_q$$
$$= b_i(0) + \eta_i(t) + \Gamma t.$$

Similarly, for $t \geq \tau$, we can express $\max_{\{b_i(t) \in \mathcal{U}^k(t)\}} b_i(t) = b_i^k(\tau) + \eta_i(t-\tau) + \Gamma(t-\tau)$, which leads straightforwardly to the robust counterpart. □

Note that, irrespective of the norm used, the RC can be expressed in the same fashion as in Eq. (9). This means that the choice of norm does not affect RHS uncertainties.

Before discussing the radiation therapy planning problem as a conic robust two-stage LP with RHS, we first discuss the role of the timing in maximizing the value of information gained from the intermediate observation.

4. Optimal observation schedule

The quality of adaptive solutions instrumentally depends on how well the anticipated evolution matches the actual realized changes over time. To be able to measure this quantity and potentially take recourse action, it is often desirable to acquire additional information during the process. In many settings, this information collection incurs a cost. In the example of medical treatments, additional diagnostic measurements may affect the progress of treatment and/or the quality of life. In maintenance scheduling, preventive actions increase immediate costs, but may reduce the failure rate and the number of emergency and more costly maintenances, hence reducing the overall costs (Rausand and Høyland, 2004). In machine repair problems, Barlow and Hunter (1960) show that a unique optimal timing solution exists only for increasing error rate functions (but not for decreasing), making preventive maintenance beneficial for the system. In fact, when maintenance makes the process as good as new, Barlow and Hunter also show the optimal repair time to be dependent on the ratio of expected time to emergency repair and time to scheduled maintenance. In general, the issue of observation timing has been discussed in the literature mainly in conjunction with specific applications. However, to our best knowledge, a general framework is not available that can be applied to a variety of applications and has the potential to provide deeper insights into some of the past results. Here, we take a first step towards such a unifying approach.

In principle, the benefits of additional information have to be measured relative to the cost of its collection. Both of these measures depend on the number of observations. To quantify the benefits coherently, we assume a constant cost and consider only one observation for the ease of exposition. The results, however, apply to an arbitrary number of observations.

The value of inferred information depends on the timing of its collection. To illustrate this dependence, consider two extreme cases, namely early and late observation. If the intermediate observation follows shortly after the initial information,

the probability of significant differences is marginal, limiting the advancement of an adapted solution over the original strategy. However, if significant differences are detected at an early stage, the adapted solution will provide benefit over an extended time horizon (the remaining process) and, hence, improve the overall performance. On the other hand, when the observation is long after the initial information, the probability of a significant difference is considerably high, allowing for a drastically improved adapted solution. However, the time window of benefit for such a late but sizable adaptation is narrow, marginalizing potential overall improvements. In short, early observation has a low probability of impact that can amount to a greater benefit, whereas late adaptation has a higher probability of improvement that can affect only a short time horizon.

To model the underlying dynamics, consider the nondecreasing quantity $g(t)$ that measures the degradation of information as a function of time t. The cumulative degradation until some time T is then given by $f(T) = \int_0^T g(t)dt$. Note that $g(t)$ can be scaled accordingly, so that $f(T)$ represents some conserved total quantity. For example, a choice of $f(T) = 1$ allows for a probability interpretation of $g(t)$, if $g(t)$ is nonnegative. In the context of reliability, $g(t)$ can be regarded as probability of failure.

Intermediate information at time $0 < \tau < T$ can be considered as resetting the degradation; i.e., when the system is observed, this new information is accurate and the degradation vanishes; i.e., the degradation time time restarts. Such a general framework can be defined as follows.

Definition 1. A piece-wise differentiable function $g(t)$ is called a *reset function*, when

$$g(t) = \begin{cases} g(t) & t < \tau \\ g(t - \tau) & t \geq \tau. \end{cases}$$

Note that other reset functions, including those with a drift, can be modeled within this framework. For the sake of simplicity, we assume complete resets. The cumulative degradation function depends now on the length of process T and the observation time via

$$f(T, \tau) = \int_0^\tau g(t)dt + \int_\tau^T g(t)dt. \tag{12}$$

The following Proposition establishes the optimal schedule for observation, whenever the information degradation function can be described by Definition 1.

Proposition 3. *For the total degradation function* $f(T, \tau) = \int_0^T g(t)dt$, *with $g(t)$ as in Definition 1 and $\frac{\partial g(0)}{\partial \tau} \geq 0$, the optimal reset schedule is equidistant if and only if $g(t)$ is nondecreasing.*

Proof. We first assume that only one reset is allowed. Each direction of the proof is shown separately:

$\rightarrow$ For the schedule $\tau = T/2$ the total degradation function is given by

$$f(T, T/2) = \int_0^{T/2} g(t)dt + \int_{T/2}^T g(t - T/2)dt$$
$$= 2 \int_0^{T/2} g(t)dt.$$

Given that $\tau = T/2$ minimizes $F(T, \tau)$, for a fixed T, the optimality conditions yield

$$\frac{\partial f(T, \tau)}{\partial \tau} = 0 \Rightarrow \quad g(T/2) = g(0),$$

$$\frac{\partial^2 f(T, \tau)}{\partial \tau^2} \geq 0 \Rightarrow \quad \frac{\partial g(T/2)}{\partial \tau} \geq \frac{\partial g(0)}{\partial \tau}. \quad (13)$$

The first condition in Eq. (13) is satisfied by Definition 1. The second condition has to hold for any value of T, constituting a nondecreasing $g(t)$.

$\leftarrow$ At τ, the total degradation in Eq. (12) can be computed in continuous time via

$$f(T, \tau) = \int_0^\tau g(t)dt + \int_0^{T-\tau} g(t)dt,$$

using the continuity of $f(T, \tau)$. The optimal reset schedule for a fixed T is obtained when the total degradation is at its minimum. This occurs when

$$\frac{\partial f(T, \tau)}{\partial \tau} = g(\tau) - g(T - \tau) = 0,$$

$$\frac{\partial^2 f(T, \tau)}{\partial \tau^2} = \frac{\partial g(\tau)}{\partial \tau} - \frac{\partial g(T - \tau)}{\partial \tau} > 0. \quad (14)$$

Since $g(t)$ is nondecreasing, the derivative is $\frac{\partial g(\tau)}{\partial \tau} > 0$, $\forall \tau$. This means, based on the symmetry of Definition 1, the optimality conditions in Eq. (14) are satisfied, when $\tau = T/2$. $\square$

Observation 1. Proposition 3 extends to $N > 1$ observations for a total degradation function $f(T, \tau_1, \tau_2, \ldots, \tau_N) = \int_0^T g(t)dt$, with $g(t)$ for each τ_i as in Definition 1.

This can be shown as follows. For $N = 2$ observations, the problem can be divided into two segments, one with length $2T/3$ and the other with $T/3$. Using Proposition 3, it can be shown that the optimal observation for the first segment ($2T/3$) is at midpoint $\tau = T/3$. The result for $N > 2$ observations follows straightforwardly by induction to be equidistant at $\tau_i = \frac{T}{N+1}i$.

This means that when equidistant observations are scheduled for intermediate information collection, their benefit is maximal, because the quality of information is the highest; i.e., the information degradation is minimal. In the context of medical diagnostics and treatments, equidistant schedules are often preferred based on mostly ad hoc rules. This result provides a theoretical basis for such choices. Furthermore, it provides a generic framework to computing optimal schedules for arbitrary reset functions, even when they deviate from Definition 1. In turn, when simulation-based results lead to optimal equidistant scheduling policies, the conclusion of the underlying function to be nondecreasing is justified. In Section 5.5, we specify these findings in the context of radiation therapy planning. When the reset function contains a drift, it will lead to a constant shift per cycle. A broader discussion of other classes of reset functions is beyond the scope of this study.

5. Hypoxia-based radiation therapy planning

Intensity modulated radiation therapy (IMRT) seeks to deliver highly conformal ionizing radiation to tumorous cells. The competing goals of minimizing the dose to surrounding critical organs and healthy tissue while delivering the clinically prescribed dose to the tumor poses an optimization problem that has been studied extensively. For further details on IMRT plan optimization, see the review by Bortfeld (2006) and the references therein.

The cell response to external radiation, also known as as radiosensitivity, becomes limited when the oxygenation is reduced. This effect is commonly referred to as hypoxia and directly affects the outcome of treatments (Bristow and Hill, 2008). PET imaging allows us to measure the partial pressure of oxygen, which determines the level of hypoxia (Fleming et al., 2015). Methodologically, hypoxia-guided treatment planning is proposed by various studies, which mostly model radiosensitivity with a constant factor and result in escalated dose values to hypoxic subvolumes (Chao et al., 2001; Alber et al., 2003; Bentzen, 2005; Thorwarth et al., 2007; Grosu et al., 2007; Lee et al., 2008; Hendrickson et al., 2011; Horsman et al., 2012). It is proposed to adjust the radiosensitivity factor to the tracer uptake observed from PET scans (Bowen et al., 2009).

Most radiation treatments are fractionated over an extended time period (typically several weeks) in order to increase the recovery probability of healthy tissue (Reinhold and Visser, 1986; Field and Hornsey, 1977). During this period, radiosensitivity may change. In fact, many concurrent treatments with chemotherapy are designed to also drive such a change. Both the treatment-induced reoxygenation and the admixtured radiosensitizing compounds enhance the effectiveness of radiation, particularly at later weeks (Okamoto et al., 2013). This also means that treatment plans based on a static radiosensitivity factor will encounter two problems: they will deliver significantly more dose than necessary at later stages; and they fail to leverage the improved oxygenation (Lin et al., 2008). More recently, re-planning methods have been proposed that take into account a changing radiosensitivity factor (Toma-Dasu et al., 2012; Malinen et al., 2006; Servagi-Vernat et al., 2015). However, re-planning methods are resource intensive, and hence, are not always clinically viable. Moreover, they can only benefit future stages of treatment based on updated data and are not anticipative; i.e., the later the re-planning occurs, the less time horizon is left for the benefits to positively impact the outcomes. On the other hand, if re-planning occurs at an early stage, the difference to initial information is negligible, marginalizing the benefits.

In this section, we provide an anticipative and time-dependent approach, leveraging a temporal radiosensitivity factor. Our goals are the following:

1. To model the uncertainty in reoxygenation via time-dependent sets, as in Eq. (11);
2. To develop a conic robust two-stage LP for the reoxygenation effect;
3. To provide a numerical computation on a clinical prostate cancer case;
4. And to empirically establish the optimal timing of information collection.

We first introduce the notation for the time-dependent model, before discussing the corresponding uncertainty set and the conic problem.

Notation: All tissues in the volume of interest are discretized into volume elements $v \in \mathcal{V}$, called voxels, belonging to four mutually exclusive sets $\mathcal{V} = \mathcal{H} \cup \mathcal{T} \cup \mathcal{C} \cup \mathcal{N}$.

Here, $\mathscr{H}$ denotes the set of hypoxic tumor voxels, $\mathscr{T}$ the set of well-oxygenated (normoxic) tumor voxels, $\mathscr{C}$ the set of critical organ voxels, and $\mathscr{N}$ the set of normal tissue voxels. Additionally, the cross-section of the beams is discretized into beamlet $b \in \mathscr{B}$. Furthermore, the radiation intensity of each beamlet is denoted as x_b and the dose absorption coefficient of voxel v, irradiated by beamlet b, as $d_{b,v}$. The dose deposited to the voxel v is calculated by $\hat{d}_v = \sum_{b \in \mathscr{B}} d_{b,v} x_b$. Since the treatment is fractionated, the dose can be divided over time t, such that $\hat{d}_v = \sum_{t=1}^{T} \sum_{b \in \mathscr{B}} d_{b,v}^t x_b^t$, leading to a multi-stage process. The radiosensitivity factor, also referred to as dose escalation factor for voxel v, is denoted by ρ_v, when it is constant, and by ρ_v^t, when it is time-dependent.

5.1. Time-dependent uncertainty set for reoxygenation

Hypoxia affects the cell response to the dose. To account for this, $d_{b,v}^t$ has to be modified by a factor, that is independent of beamlets. Therefore, a factor ρ_v is imposed on the clinically prescribed dose θ for the hypoxic subregion, forming the lower limit of $\sum_{b \in \mathscr{B}} d_{b,v}^t x_b^t \geq \underline{\theta}_v \rho_v^t$, $\forall v \in \mathscr{H}$, $\forall t$. When reoxygenation occurs, ρ_v becomes ρ_v^t. However, the functional dependence of t is unknown. Since any empirical or probabilistic knowledge about this dependence remains approximate and, hence, uncertain, we assume ρ_v^t to reside in an uncertainty set that can vary in time. As established in Section 2, a conic model provides a natural description. Note that the conic description can be further refined, when detailed knowledge about an underlying distribution or accurate measurement becomes available.

To construct the uncertainty set, we consider the period before and after the observation (e.g., using a PET scan), which shall occur at $t = \tau$. Starting at $\rho_v^1 > 1$, the reoxygenation induces $\rho_v^t = \rho_v^1 - \eta \cdot (t - 1)$, where η is an expected rate of change in reoxygenation, which remains uncertain. Once the observation occurs, an accurate value of ρ_v^τ is measured. Given the measurement and reporting tolerance (or resolution), we consider finitely many possible observed values for ρ_v^τ and denote them with $\rho_v^{\tau,k}$. Consequently, for the subsequent time periods after the observation, ρ_v^t can be described as $\rho_v^t = \rho_v^{\tau,k} - \eta \cdot (t - \tau)$. Therefore, the corresponding uncertainty cone can be expressed as,

$$\mathcal{U}^k(t)$$
$$= \left\{ \rho_v^t \mid \begin{cases} \|\rho_v^t - \rho_v^1 - \eta \cdot (t-1)\|_2 \leq \Gamma \cdot (t-1) & t < \tau, \\ \|\rho_v^t - \rho_v^{\tau,k} - \eta \cdot (t-\tau)\|_2 \leq \Gamma \cdot (t-\tau) & t \geq \tau \end{cases} \right\}.$$
(15)

In principle, the driving factors of a changing ρ_v^t can be the radiation dose, the chemotherapeutical regiment, and biological changes, all of which are additive and linear functions of time and can be captured by the uncertainty set, as in Eq. (13).

5.2. Conic robust two-stage LP for reoxygenation

Employing the uncertainty cone within the robust two-stage LP Eq. (6)), we seek to minimize the total dose over the two treatment stages with observation occurring at $t = \tau$ as

$$\min_{\mathbf{x}^k \geq 0} \sum_{v \in \mathscr{V}} \sum_{t=1}^{T} \sum_{b \in \mathscr{B}} d_{b,v}^t x_b^{t,k} \qquad (16)$$

s.t. $\sum_{b \in \mathscr{B}} d_{b,v}^t x_b^{t,k} \geq \underline{\theta}_v^t \qquad \forall v \in \mathscr{T}, \forall t \qquad (17)$

$\sum_{b \in \mathscr{B}} d_{b,v}^t x_b^{t,k} \leq \overline{\theta}_v^t \qquad \forall v \in \mathscr{T}, \forall t \qquad (18)$

$\sum_{t=1}^{T} \sum_{b \in \mathscr{B}} d_{b,v}^t x_b^{t,k} \leq \widetilde{\theta}_v \qquad \forall v \in \mathscr{C} \qquad (19)$

$\sum_{b \in \mathscr{B}} d_{b,v}^t x_b^{t,k} \geq \underline{\theta}_v^t \rho_v^{t,k} \quad \forall v \in \mathscr{H}, \ \rho_v^{t,k} \in \mathcal{U}^k(t), \forall t. \quad (20)$

The constraints in Equations (17) and (18) establish lower and upper fractionated prescribed dose limits, $\underline{\theta}_v^t = \underline{\theta}_v / T$ and $\overline{\theta}_v^t = \overline{\theta}_v / T$, to ensure tumor coverage on normoxic tumor voxels. Moreover, constraint (19) enforces the total dose to critical organ voxels to be below clinical limits $\widetilde{\theta}_v$ over the course of the treatment. The uncertain constraint (20) is imposed on hypoxic voxels such that θ_v^t is escalated by the worst-case radiosensitivity factor, $\max_{\rho_v^{t,k}} \rho_v^{t,k}$. This means, when the measurement corresponds to the k-th realization, the plan adapts to the corresponding k-th solution.

This formulation translates to the case of right-hand side uncertainty, as discussed in Section 3. The constraint in (Eq. (20)) can be expressed through the robust counterpart as,

$$\sum_{b \in \mathscr{B}} d_{b,v}^t x_b^t \geq \theta_v^t \left(\rho_v^1 - \eta \cdot (t-1) + \Gamma \cdot (t-1) \right)$$
$$\forall \quad v \in \mathscr{H}, t < \tau,$$
$$\sum_{b \in \mathscr{B}} d_{b,v}^t x_b^t \geq \theta_v^t \left(\rho_v^{\tau,k} - \eta \cdot (t-\tau) + \Gamma \cdot (t-\tau) \right)$$
$$\forall \quad v \in \mathscr{H}, t \geq \tau.$$

Implementation: To evaluate the robust model, we consider a fixed *nominal scenario* k' at $\tau = 4$ to control the additional source of uncertainty in the realization. As mentioned, the *worst-case scenario* is considered to be $\max_{\rho_v^{t,k}} \rho_v^{t,k}$. The solution from the robust model, in Equations (16–20), $\mathbf{x}^{\text{robust}}$, is compared with two specific instances; where $\rho_v^t = \rho_v^1$, $\forall v$ (no reoxygenation) and $\rho_v^t = 1$, $\forall v$ (ignoring hypoxia). Note that assuming no reoxygenation leads to the fixed dose escalation model, $\mathbf{x}^{\text{escalated}}$, which is fairly common in clinical practice for treating hypoxic tumors. Alternatively, ignoring hypoxia leads to the traditional fractionated model, with solutions $\mathbf{x}^{\text{fraction}}$. The model was implemented in Matlab (2013), using the Gurobi solver on a commercial desktop computer.

5.3. Clinical study on a prostate cancer case

The three solutions are demonstrated through a prostate cancer case (Deasy *et al.*, 2003). We simulate hypoxia on 54.4% of tumor volume, in accordance with observations from previous studies (Servagi-Vernat *et al.*, 2015). The remaining 45.6% is assumed to be well-oxygenated tumor voxels. Specifically, the number of voxels are $|\mathscr{H}| = 1337$ and $|\mathscr{T}| = 1121$. Based on a prescribed dose of 75Gy to the tumor, the thresholds are set as $\underline{\theta}_v = 70\text{Gy}$ and $\overline{\theta}_v = 95\text{Gy}$. The critical organs to spare are bladder and rectum, with limiting threshold dose $\widetilde{\theta}_v = 90\text{Gy}$ for both. The bladder consists of 3727 voxels and the rectum of 2530 voxels. Dose

absorption coefficients, $d_{b,v}^t$, are calculated using the QIB algorithm, which is based on the convolution superposition principle and assumes a low heterogeneity medium (Ahnesj, ö 1989). The coefficients were generated for five beams from angles $90°$, $125°$, $145°$, $215°$, and $245°$. Furthermore, we plan for a seven-week treatment duration, which is typical for most prostate cancer cases.

To simulate the oxygenation process, we parameterize the trajectory of ρ through the reoxygenation rate η and the uncertainty budget rate Γ based on observed values from past studies (Servagi-Vernat *et al.*, 2015; Lin *et al.*, 2008) in the following fashion. Under the nominal scenario k', approximately complete reoxygenation is assumed by the end of the treatment, leading to $\rho_v^T = 1.08$. Based on this terminal value and the initial value $\rho_v^1 = 1.25$, a rate of reoxygenation is computed as $\eta = 2.8\%$. Under the worst-case scenario, a maximum $\rho_v^T = 1.18$ is assumed, resulting in a uncertainty growth rate of $\Gamma = 1.6\%$. Under the nominal condition, $\rho_v^{\tau,k'} = 1.18$ is observed.

5.3.1. Numerical results

The quality of each of the three optimized plans, namely $\mathbf{x}^{\text{robust}}$, $\mathbf{x}^{\text{escalated}}$, and $\mathbf{x}^{\text{fraction}}$, is measured based on the three clinical criteria for the hypoxic subvolume, D_{50}, D_{95}, and equivalent uniform dose (EUD). Here, D_x is the absolute dose that is delivered to $x\%$ of volume and EUD measures dose homogeneity (Niemierko, 1997) and is computed as,

$$\text{EUD} = \left(\frac{1}{|\mathscr{H}|} \sum_{v \in (\mathscr{H})} \hat{d}_v{}^\alpha \right)^{1/\alpha},$$

where $\alpha = -10$ for tumor. We report the quality of the plans with respect to the two competing objectives, namely achieving desired dose to target while minimizing organ at risk dose. Since misalignments may degrade any fractionated therapy, we also probe the sensitivity of plans. We then summarize the overall numerical findings and their clinical implication.

Target Coverage: When evaluating plans in clinical settings with regard to tumor, D_{50} (median dose) is recommended to be equal to the prescribed dose, D_{95} is suggested at 95% of the prescribed dose, and EUD is reported as a relative deviation from the prescribed dose. We will impose the same criteria.

The tumor dose criteria are summarized in Table 1 for the three models. With regard to the three criteria, the fractionated model, on average, leads underdose to the hypoxic tumor subvolume. In comparison, the escalated model delivers a significantly higher dose. The robust model outperforms both the escalated and fractionated models and delivers a dose within 1% accuracy of the clinical criteria. Note that, in addition to this

Table 1. Plan evaluation based on clinically recommended dose criteria for tumor.

Dose Criteria [Gy]	Fractionated	Escalated	Robust
$D_{50} = 75$	66.7	78.4	75.2
$D_{95} \geq 71.3$	60.6	74.5	71.9
$EUD = 75$	65.8	78.2	75.1

Table 2. Plan evaluation based on clinically recommended dose criteria for bladder and rectum.

Structure	Dose Criteria [Gy]	Fractionated	Escalated	Robust
Bladder	$D_{30} \leq 70$	28.5	35.5	30.6
	$D_{15} \leq 80$	62.2	70.2	62.9
Rectum	$D_{20} \leq 70$	28.8	35.0	28.3
	$D_{15} \leq 75$	42.4	49.5	43.7

advantage, $\mathbf{x}^{\text{robust}}$ remains relatively insensitive, when the realized ρ^t deviates from the assumed trajectory.

Organ Sparing: The clinically recommended criteria for critical organs are D_{30} and D_{15} on the bladder as well as D_{20} and D_{15} on the rectum (Lawton *et al.*, 2009; RTOG, 2014). The evaluation of results with respect to these criteria are summarized in Table 2. The dose points of the robust model for both critical organs are below the clinically established thresholds and comparable to the fractionated method. The escalated method leads to significantly higher dose. In fact, D_{30} on the bladder in Table 2 is 177% and 173% of the fractionated and robust D_{30}, respectively. Similar trends are observed on the bladder D_{15} and rectum D_{20} and D_{15} for the escalated model.

Misalignments: They can occur between fractions and their effect may be compounded by set-up errors of the linear accelerator (gantry angle or leaf positions) (Bertsimas *et al.*, 2010a). In prostate, misalignments amount to a 1–4 mm random translation (Van Herk, 2004). To estimate the impact on dose distributions, we apply $\mathbf{x}^{\text{robust}}$, $\mathbf{x}^{\text{escalated}}$, and $\mathbf{x}^{\text{fraction}}$ to 100 randomly translated geometries and tally total dose distributions over all times.

For $\mathbf{x}^{\text{fraction}}$, when misalignments are simulated in the absence of hypoxia (nominal setting), the deviations amount to 2% of dose points. This deviation increases to 3% for hypoxic tumors. For $\mathbf{x}^{\text{robust}}$, we observe a deviation of 4% in the worst case. This showcases that robust plans are comparably forgiving to misalignments as traditional fractionated plans. Detailed analysis is available in the electronic companion. Furthermore, with regard to motion management (see, e.g., Nohadani *et al.* (2010)), these solutions are static and, in this regard, comparable to conventional settings with respect to motion uncertainty.

Summary and Clinical Implication: In general, an underdose to target can increase the likelihood of tumor survival, while excess radiation to critical organs may lead to dysfunctional organs or even secondary cancer (Schneider *et al.*, 2006). For the escalated model, we observe an overdose to the tumor and an increased dose to critical organs. Conversely, the fractionated model leads to tumor underdose, when hypoxia is not taken into account. The proposed robust model achieves improved results on the tumor by increasing dose to overcome hypoxia changes that is overlooked by the fractionated model. In addition, the robust model anticipates the reoxygenation process, thus reducing the excess dose at later fractions. In delivery, robust plans are observed to be forgiving to misalignments.

In the following, we relax the fixed nominal scenario k' and the observation time $\tau = 4$ in order to numerically evaluate the robust model over a set of possible scenarios $k \in K$ and covering the entire uncertainty cone $\tau \in [1, T]$, allowing a comparison with the theoretical results from Section 4.
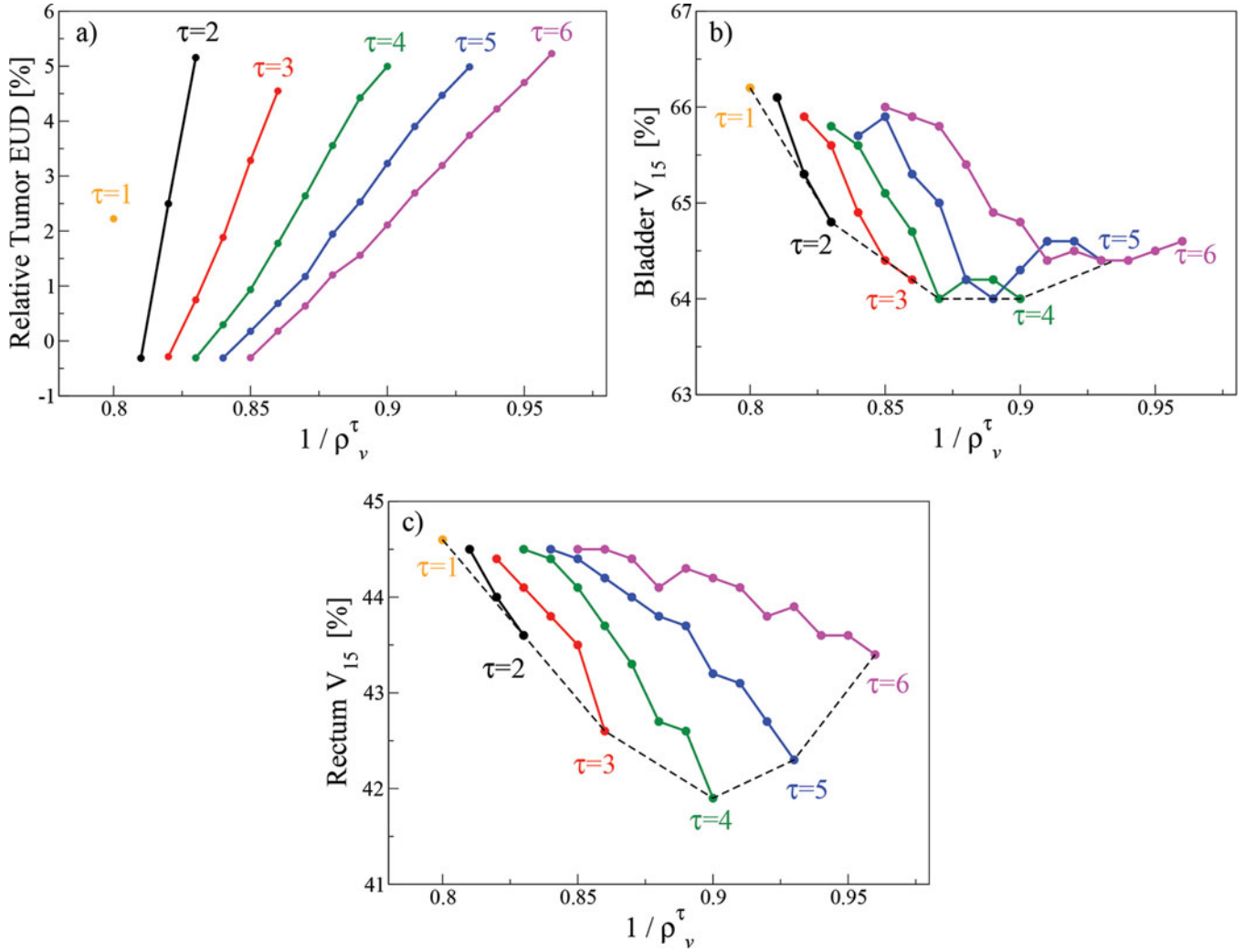
Figure 2. Changes in plan criteria with respect to observation epoch τ and radiosensitivity factor ρ_v^τ. (a) Tumor EUD relative to prescribed dose; (b) bladder V_{15}; (c) rectum V_{15}. The black dashed line connects the minima as a visual guide. Note that $1/\rho_v^\tau$ is proportional to time or fraction number.

5.4. Optimal timing of observation

Additional diagnostics to augment treatments typically incur additional cost. They also often lead to collateral effects which may reduce the quality of life, in some cases accompanied with lasting changes (e.g., CTs increase patient's exposure to radiation). Therefore, when such supplemental observations are considered, the goal ought to be to minimize their number in order to contain costs. On the other hand, updated information is more reliable, enabling more effective treatment adaptation. Consequently, when cost and collateral effects are not an issue, increased number of observations provide a near-online information, allowing for effective adaptation. Alternatively, when both cost and efficacy of treatment are considered, the resulting fixed number of observation determines the costs, while the timing of the observation determines the benefits of adaptation. In the context of radiation therapy, observation at early fractions may lead to marginal adaptations, which will lose efficacy in later stages. Conversely, adapting late could result in suboptimal plans until the observation and in a short window of benefit of adaptation. Here, we numerically explore various observation policies. The goal is to spare critical organs while maintaining clinically acceptable tumor coverage.

To observe the impact of different observation epoch τ and possible realizations of ρ_v^τ (the observed parameter), we compute robust plans for different observation times $\tau \in [1, T]$. Specifically, the possible realizations of ρ_v^τ lead to a range of $1/\rho_v^{\tau,k} = 0.8, 0.81, 0.82, \ldots, 1.0$, that lies within the uncertainty cone. Note that $1/\rho_v^{\tau,k}$ is inversely proportional to elapsing time. We first discuss the impact of τ and $1/\rho_v^{\tau,k}$ on tumor EUD before analyzing the consequences for the bladder and rectum V_{15}.

Figure 2a displays the significant increase in tumor EUD when marginally varying ρ_v^τ (steep slope). Such an increase in EUD corresponds to an increase in dose to tumor, which can be expected, since the robust model accounts for the worst case. This effect is stronger the earlier the observation occurs ($\tau \leq 4$). This is because extremely conservative uncertainty sets are assumed for later fractions, demonstrating the rapid degradation of plans when adapting early. On the other hand, later observations can lead to excess dose to tumor from early on.

For the critical organs, significant improvement is observed for bladder and rectum V_{15}, when the observation occurs at early fractions ($\tau \leq 4$) compared to later stages ($\tau > 4$) of

the treatment (see Figs. 2b and 2c at fixed $1/\rho_v^\tau$). In fact, as long as some observation occurs ($\tau > 1$), there is improvement in critical organ sparing compared to the non-adaptive case ($\tau = 1$). The plateau in bladder V_{15} towards the midpoint of the treatment shows that plan quality is independent of realized $\rho_v^{\tau,k}$ for this time span. More importantly, for both the bladder and the rectum, the lowest V_{15} occurs at $\tau = 4$, suggesting an observation around the treatment midpoint to be optimal for organ sparing. This empirical result confirms our theoretical findings in Section 4.

6. Discussion

The tractability of ARO approximations depends on the problem size, on the uncertainty set dimension, and on the number of constraints (Bertsimas and Caramanis, 2010). In fact, solving for two contingency plans based on two possible realizations is already NP-hard. This is because this two-adaptability problem requires an optimal partitioning of the uncertainty set. Moreover, the number of possible realizations of the uncertainty grows exponentially with increasing uncertainty dimensions. However, for low-dimensional problems with low-dimensional uncertainty sets, finitely adaptable frameworks can be employed.

In the case of tumor hypoxia uncertainty, as discussed in this article, the problem includes a large number of constraints, but has a low-dimensional uncertainty set. Therefore, it is possible to efficiently solve it for finitely many observations. A discretization of possible scenarios is justified, since all measurements are taken and reported in discrete units (e.g., cGy for dose or cc for volumes). Furthermore, the proposed model also allows for nonlinear functions for the dependence of the second-stage uncertainties on the first-stage decisions. The uncertainty cone constrains all trajectories (even when nonlinear) to evolve within it.

With regard to reoxygenation, its progress may vary amongst cell groups. To this end, perfusion plays a significant role, along with radiation dose and concurrent chemotherapy (Thorwarth *et al.*, 2005). These factors are beyond the scope of this work, since these are additional sources of uncertainties that would convolute the interpretation of results. However, their incorporation is straightforward, as they directly affect the trajectory of ρ^t, for which we only imposed generic assumptions. Furthermore, the use of the Euclidean norm in the IMRT problem may be extended to tailored norms for specific structures. For example, l_∞ norm may be superior for serial organs, since the maximum dose to any subvolume damages the entire structure. Alternatively, the l_1 norm may be used for parallel organs, since damage to a subvolume does not imply damage to the entire structure. For most structures, including the prostate tumor, the Euclidean norm is appropriate.

7. Conclusion

Current two-stage RO approaches consider time-invariant uncertainty sets. However, when uncertainties evolve over time, this static assumption leads to suboptimal solutions. To address this issue, we provide an RO approach based on time-dependent uncertainty sets. We develop conic robust two-stage LPs as a natural model of such time-dependent uncertainties. Robust counterparts are provided for both uncertainties in the constraint parameters and uncertainties on the right-hand side. Given that the value of adaptation depends on its timing, we also develop a general framework for optimal observation schedule, which can be applied to a broad range of applications.

A clinical radiation therapy case is discussed, where the levels of radiosensitivity are uncertain and evolve over the course of the treatment. The proposed framework incorporates changes in hypoxia and reoxygenation while significantly improving tumor control and maintaining the sparing of critical organs. Furthermore, the robust plans are also insensitive to misalignment errors that may occur during delivery, suggesting clinical relevance. Given the generic assumptions and the natural inclusion of temporal effects, this framework is well suited for a broad range of RO problems with changing uncertainties.

ORCID

Omid Nohadani 🔘 http://orcid.org/0000-0001-6332-3403

References

Ahnesjö, A. (1989) Collapsed cone convolution of radiant energy for photon dose calculation in heterogeneous media. *Medical Physics*, **16**, 577–592.

Alber, M., Paulsen, F., Eschmann, S. M., and Machulla, H. J. (2003) On biologically conformal boost dose optimization. *Physics in Medicine and Biology*, **48**, N31.

Barlow, R., and Hunter, L. (1960) Optimum preventive maintenance policies. *Operations Research*, **8**, 90–100.

Ben-Tal, A., El Ghaoui, L., and Nemirovski, A. (2009) *Robust Optimization*. Princeton University Press, Princeton, NJ.

Ben-Tal, A., Goryashko, A., Guslitzer, E., and Nemirovski, A. (2004) Adjustable robust solutions of uncertain linear programs. *Mathematical Programming*, **99**, 351–376.

Ben-Tal, A., and Nemirovski, A. (1999) Robust solutions of uncertain linear programs. *Operations Research Letters*, **25**, 1–13.

Bentzen, S. M. (2005) Theragnostic imaging for radiation oncology: Dose-painting by numbers. *The Lancet Oncology*, **6**, 112–117.

Bertsimas, D., Brown, D. B., and Caramanis, C. (2011) Theory and applications of robust optimization. *SIAM Review*, **53**, 464–501.

Bertsimas, D., and Caramanis, C. (2010) Finite adaptability in multistage linear optimization. *IEEE Transactions on Automatic Control*, **55**, 2751–2766.

Bertsimas, D., Nohadani, O., and Teo, K. M. (2010a) Nonconvex robust optimization for problems with constraints. *INFORMS Journal on Computing*, **22**, 44–58.

Bertsimas, D., Nohadani, O., and Teo, K. M. (2010b) Robust optimization for unconstrained simulation-based problems. *Operations Research*, **58**, 161.

Bertsimas, D., Pachamanova, D., and Sim, M. (2004) Robust linear optimization under general norms. *Operations Research Letters*, **32**, 510–516.

Birge, J. R., and Louveaux, F. (2011) *Introduction to Stochastic Programming*. Springer Verlag, New York.

Bortfeld, T. (2006) IMRT: A review and preview. *Physics in Medicine and Biology*, **51**, R363.

Bowen, S. R., Flynn, R. T., Bentzen, S. M., and Jeraj, R. (2009) On the sensitivity of IMRT dose optimization to the mathematical form of a biological imaging-based prescription function. *Physics in Medicine and Biology*, **54**, 1483.

Bristow, R. G., and Hill, R. P. (2008) Hypoxia and metabolism: Hypoxia, DNA repair and genetic instability. *Nature Reviews Cancer*, **8**, 180–192.

Calafiore, G., and Campi, M. C. (2005) On two–stage portfolio allocation problems with affine recourse. *44th IEEE Conference on Decision and Control, 2005 and 2005 European Control Conference, CDC–ECC'05*. IEEE, 8042–8047.

Chao, K. S. C., Bosch, W. R., Mutic, S., Lewis, J. S., Dehdashti, F., Mintun, M. A., Dempsey, J. F., Perez, C. A., Purdy, J. A., and Welch, M. J. (2001) A novel approach to overcome hypoxic tumor resistance: Cu–ATSM–guided intensity–modulated radiation therapy. *International Journal of Radiation Oncology* Biology* Physics*, **49**, 1171–1182.

Dantzig, G. B. (1955) Linear programming under uncertainty. *Management Science*, **1**, 197–206.

Dantzig, G. B., and Madansky, A. (1961) On the solution of two–stage linear programs under uncertainty. *Proceedings of the Fourth Berkeley Symposium on Mathematical Statistics and Probability*, vol. 1. University of California Press Berkeley, CA, 165–176.

Deasy, J. O., Blanco, A. I., and Clark, V. H. (2003) CERR: A computational environment for radiotherapy research. *Medical Physics*, **30**, 979–985.

Field, S. B., and Hornsey, S. (1977) Repair in normal tissues and the possible relevance to radiotherapy. *Strahlentherapie*, **153**, 371–379.

Fleming, I. N., Manavaki, R., Blower, P. J., West, C., Williams, K. J., Harris, A. L., Domarkas, J., Lord, S., Baldry, C., and Gilbert, F. J. (2015) Imaging tumour hypoxia with positron emission tomography. *British Journal of Cancer*, **112**, 238–250.

Grosu, A., Souvatzoglou, M., Röper, B., Dobritz, M., Wiedenmann, N., Jacob, V., Wester, H., Reischl, G., Machulla, H., Schwaiger, M., et al. (2007) Hypoxia imaging with FAZA–PET and theoretical considerations with regard to dose painting for individualization of radiotherapy in patients with head and neck cancer. *International Journal of Radiation Oncology* Biology* Physics*, **69**, 541–551.

Guslitser, E. (2002) Uncertainty–immunized solutions in linear programming. Ph.D. thesis, Technion–Israel Institute of Technology.

Hendrickson, K., Phillips, M., Smith, W., Peterson, L., Krohn, K., and Rajendran, J. (2011) Hypoxia imaging with [F–18] FMISO–PET in head and neck cancer: Potential for guiding intensity modulated radiation therapy in overcoming hypoxia–induced treatment resistance. *Radiotherapy and Oncology*, **101**, 369–375.

Horsman, M. R., Mortensen, L. S., Petersen, J. B., Busk, M., and Overgaard, J. (2012) Imaging hypoxia to improve radiotherapy outcome. *Nature Reviews Clinical Oncology*, **9**, 674–687.

Lawton, C. A. F., Michalski, J., El-Naqa, I., Buyyounouski, M. K., Lee, W. R., Menard, C., O'Meara, E., Rosenthal, S. A., Ritter, M., and Seider, M. (2009) RTOG GU radiation oncology specialists reach consensus on pelvic lymph node volumes for high-risk prostate cancer. *International Journal of Radiation Oncology* Biology* Physics*, **74**, 383– 387.

Lee, N. Y., Mechalakos, J. G., Nehmeh, S., Lin, Z., Squire, O. D., Cai, S., Chan, K., Zanzonico, P. B., Greco, C., Ling, C. C., et al. (2008) Fluorine–18–labeled fluoromisonidazole positron emission and computed tomography–guided intensity–modulated radiotherapy for head and neck cancer: A feasibility study. *International Journal of Radiation Oncology* Biology* Physics*, **70**, 2–13.

Lin, Z., Mechalakos, J., Nehmeh, S., Schoder, H., Lee, N., Humm, J., and Ling, C. C. (2008) The influence of changes in tumor hypoxia on dose-painting treatment plans based on 18F-FMISO positron emission tomography. *International Journal of Radiation Oncology* Biology* Physics*, **70**, 1219–1228.

Lorca, A., and Sun, X. A. (2015) Adaptive robust optimization with dynamic uncertainty sets for multi–period economic dispatch under significant wind. *IEEE Transactions on Power Systems*, **30**, 1702–1713.

Malinen, E., Søvik, A., Hristov, D., Bruland, Ø. S., and Olsen, D. R. (2006) Adapting radiotherapy to hypoxic tumours. *Physics in Medicine and Biology*, **51**, 4903.

Mani, M., Sing, A. K., and Orshansky, M. (2006) Joint design–time and post–silicon minimization of parametric yield loss using adjustable robust optimization. *Proceedings of the 2006 IEEE/ACM International Conference on Computer–Aided Design*, San Jose, CA. ACM, 19–26.

Men, H., Freund, R. M., Nguyen, N. C., Saa-Seoane, J., and Peraire, J. (2014) Fabrication–adaptive optimization with an application to photonic crystal design. *Operations Research*, **62**, 418–434.

Mudchanatongsuk, S., Ordóñez, F., and Liu, J. (2008) Robust solutions for network design under transportation cost and demand uncertainty. *Journal of the Operational Research Society*, **59**, 652–662.

Niemierko, A. (1997) Reporting and analyzing dose distributions: A concept of equivalent uniform dose. *Medical Physics*, **24**, 103–110.

Nohadani, O., Seco, J., and Bortfeld, T. (2010) Motion management with phase-adapted 4d-optimization. *Physics in Medicine and Biology*, **55**, 5189.

Okamoto, S., Shiga, T., Yasuda, K., Magota, K., Kasai, K., Kuge, Y., Shirato, H., and Tamaki, N. (2013) Serial changes of hypoxia in head and neck cancer by fractionated radiotherapy with IMRT. *Journal of Nuclear Medicine*, **54**, 454–454.

Ordóñez, F., and Zhao, J. (2007) Robust capacity expansion of network flows. *Networks*, **50**, 136–145.

Rausand, M., and Høyland, A. T. (2004) *System Reliability Theory: Models, Statistical Methods, and Applications*, vol. 396. John Wiley & Sons, Inc., Hoboken, NJ.

Reinhold, H. S., and Visser, A. G. (1986) Multiple fractions per day in retrospect: The LQ model and the tolerance profile. *Radiotherapy and Oncology*, **5**, 259–264.

RTOG (2014) Radiation Therapy Oncology Group 0415 trial: A phase III randomized study of hypofractionated 3D-CRT/IMRT versus conventionally fractionated 3D-CRT/IMRT in patients with favorable–risk prostate cancer. www.rtog.org

Schneider, U., Lomax, A., Pemler, P., Besserer, J., Ross, D., Lombriser, N., and Kaser-Hotz, B. (2006) The impact of IMRT and proton radiotherapy on secondary cancer incidence. *Strahlentherapie und Onkologie*, **182**, 647–652.

Servagi-Vernat, S., Differding, S., Sterpin, E., Hanin, F., Labar, D., Bol, A., Lee, J. A., and Grgoire, V. (2015) Hypoxia-guided adaptive radiation dose escalation in head and neck carcinoma: A planning study. *Acta Oncologica*, **54**, 1008–1016.

Shapiro, A., and Nemirovski, A. (2005) On complexity of stochastic programming problems. *Continuous Optimization*. Springer, USA, 111–146.

Thorwarth, D., Eschmann, S., Paulsen, F., and Alber, M. (2007) Hypoxia dose painting by numbers: A planning study. *International Journal of Radiation Oncology* Biology* Physics*, **68**, 291–300.

Thorwarth, D., Eschmann, S., Scheiderbauer, J., Paulsen, F., and Alber, M. (2005) Kinetic analysis of dynamic 18F-fluoromisonidazole PET correlates with radiation treatment outcome in head–and–neck cancer. *BMC Cancer*, **5**, 152.

Toma-Dasu, I., Uhrdin, J., Antonovic, L., Dasu, A., Nuyts, A., Dirix, P., Haustermans, K., and Brahme, A. (2012) Dose prescription and treatment planning based on FMISO–PET hypoxia. *Acta Oncologica*, **51**, 222–230.

Van Herk, M. (2004) Errors and margins in radiotherapy. *Seminars in Radiation Oncology*, **14**, 52–64.

Appendix: Misalignments in IMRT delivery

Misalignments are random errors and, in prostate, amount to a 1–4 mm translation. Therefore, we generated 100 randomly translated geometries in each spatial direction following a normal distribution with zero mean and 4 mm standard deviation to capture a wide range of possible scenarios. The voxel size of 1 mm × 1 mm × 5 mm warrants that such perturbations can

have a practical and measurable impact. To probe the sensitivity, the optimal solutions $\mathbf{x}^{\text{fraction}}$, $\mathbf{x}^{\text{robust}}$, $\mathbf{x}^{\text{escalated}}$ were applied to these randomly misaligned geometries. The overall dose distributions were computed voxel-wise and summarized in Table A1 for the hypoxic tumor subvolume and in Table A2 for the critical organs.

The relative range can be computed by dividing the ranges in Tables A1 and A2 by the corresponding unperturbed values in Tables 1 and 2, respectively. We observe that the relative ranges of the fractionated and robust plans are comparable to each other, suggesting that misalignments impact all three optimal plans in a similar fashion, which can be considered as forgiving.

Table A1. Impact of misalignment: The range of dose to tumor.

Dose Criteria [Gy]	Fractionated	Escalated	Robust
$D_{50} = 75$	[66.2, 67.1]	[77.0, 78.4]	[74.0, 75.1]
$D_{95} \geq 71.3$	[58.8, 63.0]	[68.9, 74.4]	[65.7, 71.8]
$EUD = 75$	[63.3, 66.5]	[74.3, 77.9]	[70.8, 74.7]

Table A2. Impact of misalignment: The range of dose to bladder and rectum.

Structure	Dose Criteria [Gy]	Fractionated	Escalated	Robust
Bladder	$D_{30} \leq 70$	[19.2, 39.7]	[27.5, 48.7]	[20.3, 40.7]
	$D_{15} \leq 80$	[51.8, 67.1]	[62.3, 73.9]	[53.3, 68.1]
Rectum	$D_{20} \leq 70$	[13.1, 43.9]	[16.9, 50.1]	[13.4, 46.5]
	$D_{15} \leq 75$	[21.5, 57.8]	[28.9, 64.3]	[22.8, 60.7]